PNAS RESEARCH ARTICLE | MICROBIOLOGY OPEN ACCESS

The F pilus serves as a conduit for the DNA during conjugation between physically distant bacteria

Kelly Goldlust[a], Adrien Ducret[a], Manuel Halte[b], Annick Dedieu-Berne[a], Marc Erhardt[b,c], and Christian Lesterlin[a,1]

Edited by Alan Grossman, Massachusetts Institute of Technology, Cambridge, MA; received June 28, 2023; accepted September 27, 2023

Horizontal transfer of F-like plasmids by bacterial conjugation is responsible for disseminating antibiotic resistance and virulence determinants among pathogenic Enterobacteriaceae species, a growing health concern worldwide. Central to this process is the conjugative F pilus, a long extracellular filamentous polymer that extends from the surface of plasmid donor cells, allowing it to probe the environment and make contact with the recipient cell. It is well established that the F pilus can retract to bring mating pair cells in tight contact before DNA transfer. However, whether DNA transfer can occur through the extended pilus has been a subject of active debate. In this study, we use live-cell microscopy to show that while most transfer events occur between cells in direct contact, the F pilus can indeed serve as a conduit for the DNA during transfer between physically distant cells. Our findings enable us to propose a unique model for conjugation that revises our understanding of the DNA transfer mechanism and the dissemination of drug resistance and virulence genes within complex bacterial communities.

horizontal gene transfer | bacterial conjugation | F Pilus | drug resistance dissemination

Significance

This study provides direct evidence of DNA transfer through the extended pilus, resolving a 60-y-old debate. It reshapes the prevailing model for F-like plasmids conjugation and significantly advances our understanding of the dissemination of drug resistance and virulence in bacterial communities.

Bacterial conjugation is a contact-dependent horizontal gene transfer mechanism that plays a crucial role in the evolution of bacterial genomes and the dissemination of metabolic properties, such as resistance to antibiotics, heavy metals, and virulence (1–5). Paradigmatic examples are members of the conjugative F plasmid family, which are highly transmissible and prevalent among clinical isolates of enterobacterial pathogens, including *Escherichia coli*, *Klebsiella pneumoniae, Salmonella enterica,* and *Shigella flexneri* (6–8). Conjugative transfer of F-like plasmids requires a Type-IV secretion system (T4SS) that transports the single-stranded DNA (ssDNA) plasmid through the cell envelope and produces the conjugative pilus, which is also strictly essential for conjugation. The structure and function of F-like conjugative pili have been extensively studied, particularly those encoded by the F and the pED208 plasmids. The F pilus is an assembly of thousands of TraA pilin (VirB2) monomers polymerized into a long, flexible, and tubular helical filament 87 Å in width and an average ~1 to 2 µm in length, which extends from the surface of the donor cells (9–13). Notably, the pilus is a highly dynamic structure that undergoes cycles of extension and retraction (14–17). The function of retraction and its requirement for conjugation have been actively debated. Using live-cell imaging of the F pilus labeled with fluorescent R17 bacteriophages, Clarke et al. (15) showed that the F pilus randomly extends and retracts to scan the host cell's surroundings to make contact with a recipient cell. The subsequent retraction of the pilus establishes physical contact between the donor and recipient cells, thereby allowing the stabilization of the mating pair through interaction between the donor's outer membrane protein TraN, and the recipient's outer membrane protein OmpA (18–21). However, whether the extended pilus can serve as a conduit for the DNA during conjugation between cells that are physically distant remains an open question. This possibility was first proposed by Charles C. Brinton 60 y ago (22, 23) and has since been a subject of extensive debate.

Little experimental evidence exists that supports the possibility of DNA transport through the extended pilus. Harrington and Rogerson (24) reported conjugation between donor and recipient cell cultures separate by a filter 6 µm thick with pores 0.01 to 0.1 µm in diameter. Using live-cell microscopy and an elegant reporter system for DNA transfer, work by Babić et al. (25) provides evidence for DNA acquisition by recipients that are not in direct contact with a donor cell. However, their experimental setup could not exclude the possibility that conjugation had occurred in the conjugation mix before imaging and the extended pilus between donor and recipient cells was not visualized. The lack of direct evidence for distant transfer favoured the currently prevailing model that conjugation strictly requires tight contact between donor and recipient cells and the possibility that the DNA passes through the pilus lumen remains speculative. In this study, we developed a real-time fluorescence microscopy approach to perform direct visualization of the fluorescently labeled F pilus (16) and the transferred DNA during conjugation in live-cells (26, 27). Our results unequivocally

Author affiliations: [a]Molecular Microbiology and Structural Biochemistry, Université Lyon 1, CNRS, Inserm, UMR5086, Lyon 69007, France; [b]Institute for Biology/Molecular Microbiology, Humboldt-Universität zu Berlin, Berlin 10115, Germany; and [c]Max Planck Unit for the Science of Pathogens, Berlin 10117, Germany

Preprint server: BioRxiv DOI: https://doi.org/10.1101/2023.06.21.545889.

Author contributions: K.G., M.H., and A.D.-B. performed research; A.D. contributed new reagents/analytic tools; K.G., A.D., M.H., and C.L. analyzed data; K.G. prepared the initial figures; M.E. prodided supervision and funding to Manuel Halte; C.L. designed research, provided supervision and funding; and M.E. and C.L. wrote the paper.

The authors declare no competing interest.

This article is a PNAS Direct Submission.

[1]To whom correspondence may be addressed. Email: Christian.lesterlin@ibcp.fr.

This article contains supporting information online at https://www.pnas.org/lookup/suppl/doi:10.1073/pnas.2310842120/-/DCSupplemental.

Published November 14, 2023.

demonstrate that the F pilus has a dual function in establishing cell-to-cell contact and serving as a conduit for DNA during transfer between physically distant cells.

Results

Cell Piliation and F Pilus Morphology. The labeling of the F pilus was performed in the wild-type (*wt*) *E. coli* K12 MG1655 strain carrying the full-length F plasmid and an expression plasmid (p *traA*^{S54C}) coding for a mutant TraA^{S54C} pilin where the surface-exposed serine 54 was substituted by a cysteine for bioconjugation with Alexa Fluor-Maleimide (AF-Mal) (Fig. 1*A*) (16). This *wt E. coli*/F/p *traA*^{S54C} partial diploid strain produces both the *wt* TraA and the mutant TraA^{S54C} pilins and exhibits conjugation efficiency comparable to the *wt* F+ donor, both in the presence or the absence of maleimide labeling (*SI Appendix*, Fig. S1*A*). Live-cell fluorescence microscopy imaging of the *wt* F/p *traA*^{S54C} strain after incubation with AF-Mal^{488} revealed efficient fluorescent labeling of the F pilus at the surface of the cells (Fig. 1*B*). To detect pili and determine their geometrical properties and their localization along the medial axis of the cell or the cell periphery, we developed a fiber-detection approach in MicrobeJ (28), a plugin for ImageJ (Fig. 1*B*, *SI Appendix*, Fig. S1*B*, and Movie S1).

Analysis of snapshot microscopy images reveals that the number of pili per cell ranges from 0 to 5 (n = 590), with the majority of piliated cells harboring one pilus or two pili (46.7% and 19.7% of the cell population, respectively) (Fig. 1*C*). The number of pili per cell slightly increases from 1.9 ± 1.2 in to 2.7 ± 1.7 (n = 647) as the cell progresses through the cell cycle from newborn to predividing cells (Fig. 1*D*). Analysis of pili length distribution shows that most pili are smaller than 2 µm in length and rarely exceed 4 µm, with an average length of 1.05 ± 0.92 µm (n = 647) (Fig. 1*E*). There is no significant correlation between the pili length and the number of pili per cells or the cell size (*SI Appendix*, Fig. S1 *C* and *D*), indicating that the cells produce pili of similar length throughout the cell cycle, regardless of the number of pili per cell. This description of cell piliation is in good agreement with previous works using either maleimide bioconjugation (13), or fluorescent MS2 (29) or R17 (15) phages to label the F pilus, thus validating our labeling procedure and analysis methods.

Using the data of 647 pili detections originating from 387 donor cells allowed us to construct a 2D density map illustrating the averaged localization of F pili around the cells (Fig. 1*F*). We observe that pili are anchored throughout the entire cell periphery, with a notable preference for the proximity of the midcell region, while anchoring at the cell tip are much less frequent (Fig. 1*G*). This positioning pattern remains consistent throughout the growth of the cells, as it is equally observed in both smaller (< 4 µm) and larger (≥ 4 µm) cells (*SI Appendix*, Fig. S1 *E–H*). Pili detection also provides insights into their flexible nature in vivo. When the pili are shorter than 0.6 µm, they project orthogonally and straight from the cell surface. However, as the pili grow longer, they progressively exhibit a more pronounced apparent curvature (Fig. 1*H*). The number, length, and curvature of pili likely are key factors that determine the donor cell's ability to probe its immediate surroundings. The 2D density map depicting the localization of pili enables us to delineate a three-dimensional space encompassing the donor cell that will be efficiently explored by the pili tips (dashed orange line in Fig. 1*F*). Analysis reveals that the majority of pili tips (594 out of 643) are confined within a 137.4-µm^3 volume, facilitating highly efficient probing within this region. Outside of this volume, probing becomes dependent on the relatively infrequent occurrence of larger pili (53 out of 643) and is therefore predicted to be much less efficient.

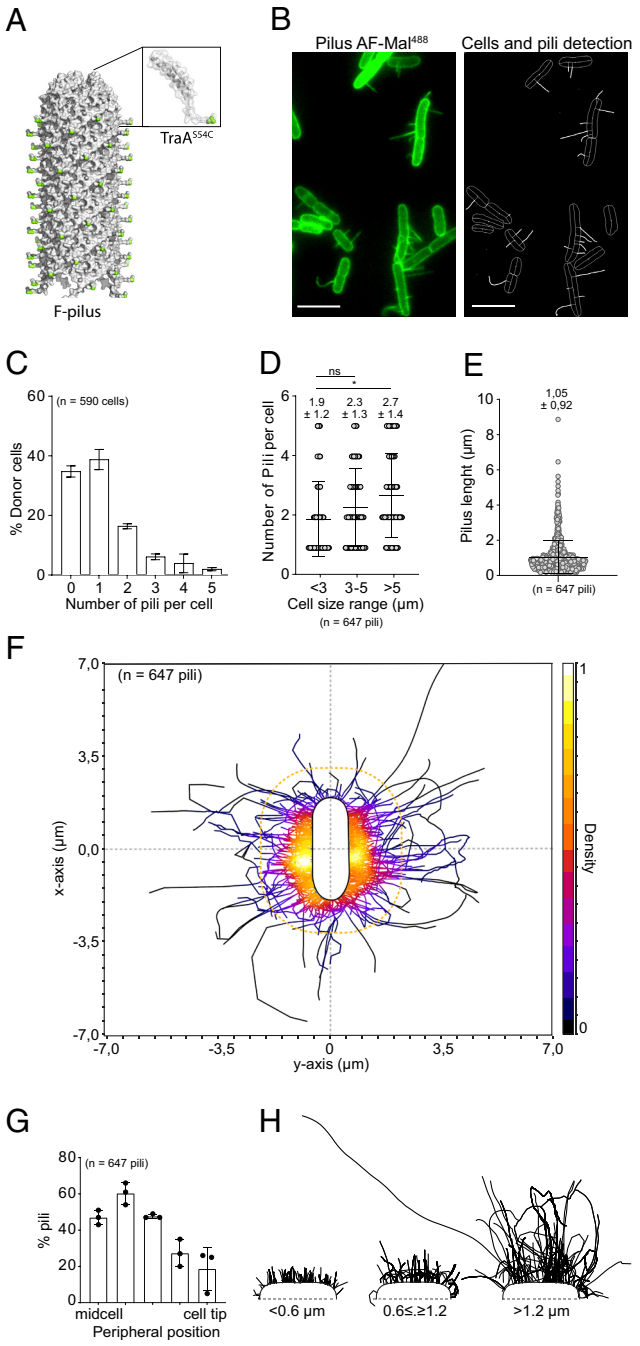

Fig. 1. Characterization of donor cells piliation. (*A*) Surface representation map of the Cryogenic electron microscopie (cryo-EM) structure of the conjugative F-pilus (adapted from ref. 12) to which the surface-exposed serine 54 (serine 3 of the mature pilin) replaced by a cysteine in the TraA^{S54C} mutant was added and displayed in green. The inset shows the structure of an individual TraA pilin to which the N-terminal carrying the serine 54 was added. (*B*) Microscopy image showing pili labeled with AF-Mal^{488} at the surface of F donor cells (*Left*) and the corresponding detection of the cells outlines and fluorescent pili using MicrobeJ custom plugin (*Right*). (*C*) Histogram of the number of pili per cells. The Mean and SD were calculated from the indicated number (n) of cells from three independent experiments. (*D*) Dot-plot of the number of pili per cell sorted by cell length range. Each open circle represents one cell. The Mean and SD were calculated from the indicated number of pili from three independent experiments. *P-value* significance from Mann–Whitney two-sided statistical test is indicated by n.s (nonsignificant) and *($P \leq 0.015$). (*E*) Dot-plot of pili length distribution in the F donor population. Mean and SD were calculated from the indicated number of Pili from three independent snapshot microscopy experiment (*F*) Two dimension (2D) density map of pili localization around the cell periphery normalized by the cell length. The number of pili (n) from three biological replicates is indicated. Density scale on the *Left*. (*G*) Histogram of pili distribution along the cell perimeter from midcell to the cell tip. (*H*) Representation of the curvature of pili categorized by size range.

F Pilus Dynamics. Next, we performed time-lapse imaging in a microfluidics chamber to visualize the real-time dynamics of F pili at the surface of donor cells in the absence of recipient cells. Using acquisition with 1 or 3 min/frame intervals, we observe that the number of pili per cell varies rapidly (Movies S1 and S2). Cells initially lacking pili in the first frame of the time-lapse were often able to produce pili within minutes (Movie S2), suggesting that most, if not all, donor cells have the capability to generate pili. Some pili appear or disappear between two consecutive frames, while others remain extended for more than 60 min (Movie S3). To capture the dynamics of pilus extension and retraction with better time resolution at the single-cell level, we acquired images with 10 s/frame intervals (Fig. 2*A* and Movie S4). Analysis of isolated extension and retraction events reveals an average 49.5 ± 50 nm/s (n = 238) extension rate, remarkably similar to the average 47.5 ± 45 nm/s (n = 275) retraction rate (Fig. 2*B* and Movie S5). These results differ from those observed with F pili labeled with fluorescent R17 phages, which exhibited a retraction rate (15 nm/s) much slower than the extension rate (39 nm/s), likely accounted for alteration of the pilus retraction by the binding of the phage (15). Live-cell imaging also exposes the rapid switching between pili extension and retraction (Movie S4). Notably, repetitive extension–retraction events are frequently observed at specific positions along the cell periphery, suggesting that multiple pili can be successively produced by the same T4SS (Movie S4). This observation raised the question of whether reversal events occur at a specific pilus size or with a definite time periodicity. To address this question, we measured the length of the pili when they switch from extension to retraction (Fig. 2*C*). We observed that the distribution of pili lengths at the onset of retraction is not statistically different to that of the whole pili population (compare Fig. 2*C* to Fig. 1*E*), indicating that retraction occurs at any pilus length. Next, we measured an average 26.7 ± 13 s (n = 215) time lag between extension and retraction events, with widespread individual data points (Fig. 2*D*). These findings suggest that the events of pilus reversal exhibit significant variability in terms of both length and timing. This supports the notion that the transitions from extension to retraction during pilus biogenesis are more likely to be random rather than precisely regulated by an internal clock.

All together, these observations indicate that the heterogeneity observed in the number and length of pili within the donor population reflects a dynamic equilibrium resulting from the rapid processes of extension, retraction, and reversal events at the single-cell level. The highly dynamic nature of pilus biogenesis, coupled with the inherent pilus flexibility, likely serves to optimize the probing ability of the donor cells in their search for a suitable attachment surface. It is worth noting that we consistently observe attachment of the pilus to the PDMS surface of the microfluidic chamber (Movie S6). Furthermore, we observe efficient attachment of the pilus to other donor cells (Movie S7), resulting in the formation of cell aggregates (Movie S8). We can note that attachment events are not necessarily followed by pilus retraction. These observations highlight the sticky property of the pili tips, enabling them to interact with biotic as well as abiotic surfaces. They also support the notion that exclusion mechanisms do not hinder the initial stages of attachment of extended pili, which in turn may explain the relatively low but consistently occurring frequency of plasmid transfer between donor cells (18, 30). Instead, exclusion likely acts later in the conjugation process, possibly after pilus retraction or at the initiation of DNA transfer.

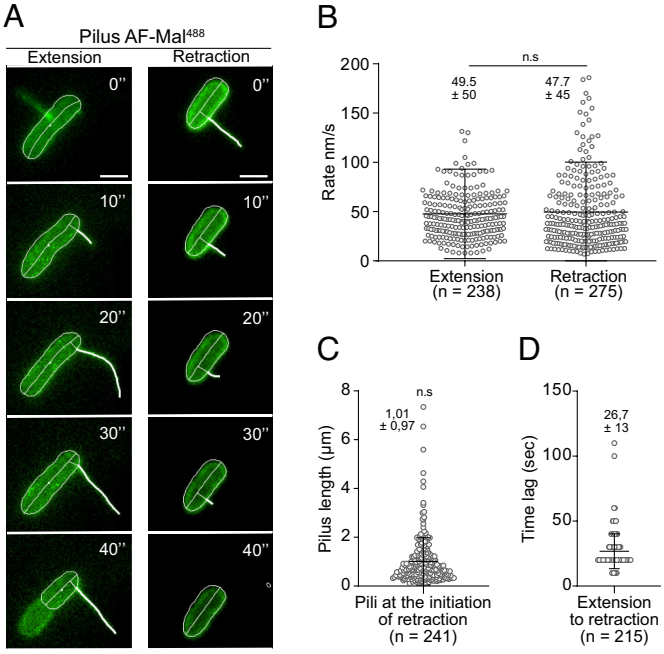

Fig. 2. Extension and retraction dynamics of the F pilus. (*A*) Time-lapse microscopy image (10 s/frame) of dynamic extension (on the *Left*) and retraction (on the *Right*) of the F pili. The contour made by the automatic detection of the plugin in MicrobeJ is represented in white. (Scale bar 1 µm.) (*B*) Jitter plot representing the speed of extension and retraction of the F pili in nm/s. Retraction and extension events analyzed using 10 s/frame time-lapse. The Mean and SD was calculated from the indicated number of retraction/extension events. *P-value* significance from Mann–Whitney two-sided statistical test is indicated by n.s (nonsignificant, $P = 0.13$). (*C*) Distribution of the pili length at the initiation of a retraction. The Mean and SD was calculated from the indicated number of pili reversal events. *P-value* significance from Mann–Whitney two-sided statistical test compared to the distribution length of all pili in the donor population (Fig. 1*E*) is indicated by n.s (nonsignificant, $P = 0.14$). (*D*) Dot-plot showing the time lag (s) between extension and retraction events. The Mean and SD was calculated from the indicated (n) number of reversal events.

DNA Transfer through Extended F Pili. To characterize the dynamics of the F pilus during conjugation, we combined F pilus labeling with reporters systems previously developed to monitor plasmid transfer using real-time microscopy (16, 26, 27). The precise moment of ssDNA plasmid transfer from donor to recipient was captured using a fluorescent protein fusion of the chromosomally encoded single-strand-binding protein Ssb (Ssb-YPet) (31). During vegetative growth, Ssb-YPet forms discrete replicative foci associated with the replication forks and located at the cell's quarter positions. However, during conjugation, Ssb-YPet forms bright membrane-associated conjugation foci revealing the presence of single-strand plasmid DNA on both sides of the conjugation pore (27). The conversion of the ssDNA plasmid into dsDNA is a hallmark for successful acquisition of the plasmid by the recipient cell and can be visualized by binding of mCherry-ParB (mCh-ParB) to a dsDNA *parS* site located on the plasmid, resulting in a fluorescent focus formation (16, 26, 27).

We performed time-lapse microscopy imaging (3 min/frame intervals) of conjugation mixes between $TraA^{S54C}$-producing *E. coli* F donors prelabeled with maleimide ($AF\text{-}Mal^{488}$ or $AF\text{-}Mal^{594}$) and recipient cells (Fig. 3 *A*–*C*). Loading of the conjugation mix within the microfluidic chamber results in microscopy fields of view with a monolayer of bacteria where most cells are in contact with other cells. Consequently, the vast majority of conjugation events observed occur between donor and recipient cells that are in tight cell-to-cell contact. The dynamics of the ssDNA transfer between cells in direct contact has been previously described by Couturier et al. (27). In the present study, we focused on conjugation events where donor and recipient cells were physically distant but connected via an extended F pilus.

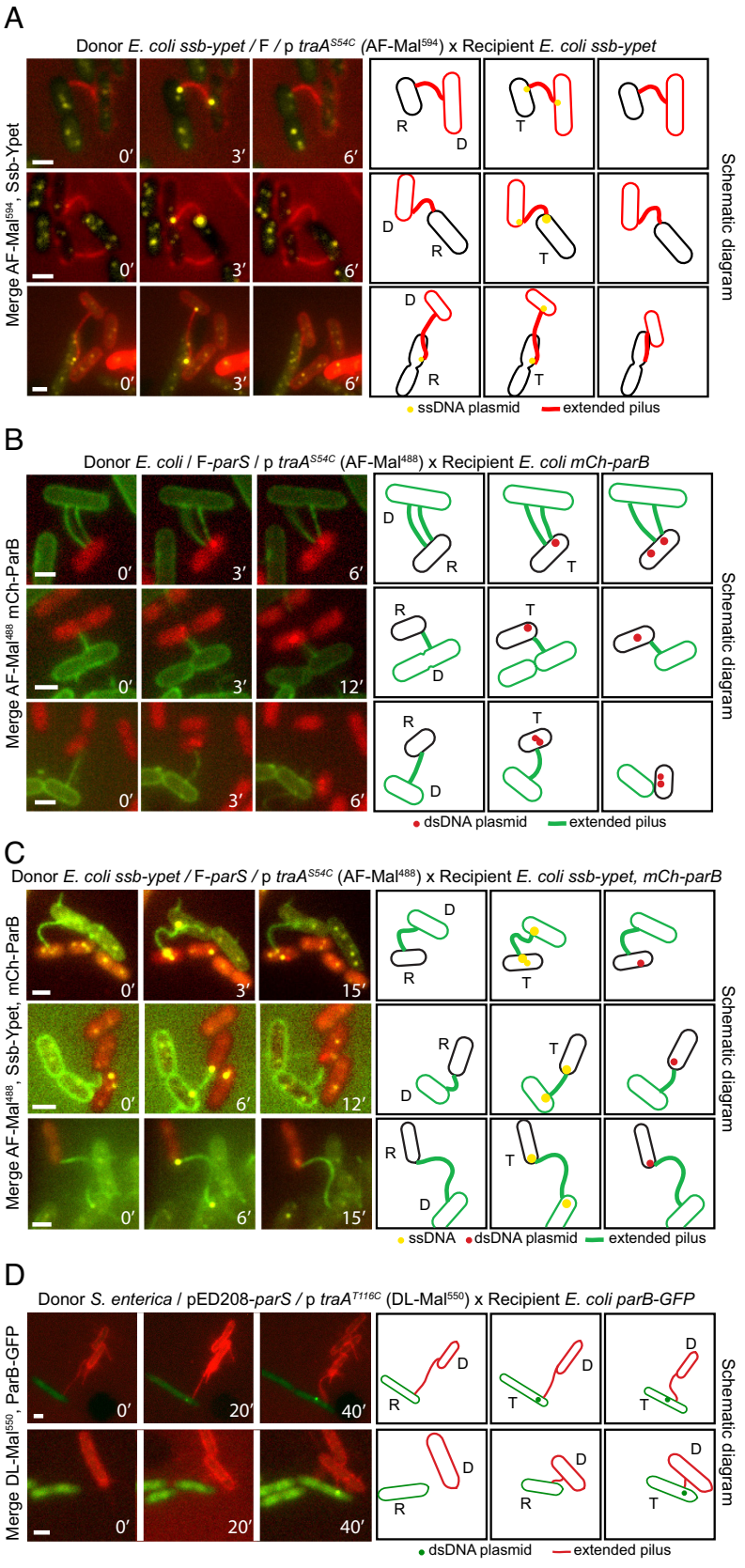

Fig. 3. Plasmid transfer between physically distant cells. (*A*) Time-lapse images of distant plasmid transfer events between *E. coli ssb-ypet*/F/p *traA*^{S54C} donors labeled with AF-Mal^{594} and *E. coli ssb-ypet* recipient cells. Distant transfer is reported by the simultaneous formation of bright membrane-proximal Ssb-Ypet conjugative foci at each edge of the pilus connecting the mating pair cells. (*B*) Time-lapse images of distant transfer events between *wt E. coli* / F-*parS*/p *traA*^{S54C} donors labeled with AF-Mal^{488} and *E. coli* recipients producing mCh-ParB. Distant transfer is reported by the formation of mCh-ParB foci confirming the acquisition of the dsDNA plasmid by the recipient cell. (*C*) Time-lapse images of distant transfer events between *wt E. coli ssb-ypet*/F-*parS*/p *traA*^{S54C} donors labeled with AF-Mal^{488} and *E. coli ssb-ypet* recipients producing mCh-ParB. Distant transfer is reported by both the formation Ssb-Ypet conjugative foci at each edge of the pilus connecting the mating pair cells and the subsequent the formation of mCh-ParB foci, which confirms the acquisition of the dsDNA plasmid by the recipient cell. (*D*) Time-lapse images of distant transfer events between *S. enterica*/pED208/p *traA*^{T116C} donor cells labeled with DayLight-Mal^{550} (DL-Mal^{550}) and *wt E. coli* recipient cells production ParB-GFP. (*A–D*: Scale bar 1 μm.) Time-lapse images (*Left*) are accompanied with corresponding schematic diagrams (*Right*) emphasizing the extended pilus and the Ssb-Ypet or mCh-ParB foci associated with the transferred ssDNA and the dsDNA plasmid in the recipient cells.

First, we examined Ssb-Ypet dynamics in recipients and donors labeled with AF-Mal^{594} to covisualize the transferred ssDNA plasmid together with the F pilus (Fig. 3*A*, *SI Appendix*, Fig. S2*A*, and Movie S9). Analysis of the time-lapse images reveals distant ssDNA transfer events as determined by the simultaneous formation of bright membrane-associated Ssb-Ypet conjugative foci in the mating pair cell. These Ssb-Ypet foci are precisely located at both ends of the pilus, corresponding to the anchoring and the attachment point of the pilus on the donor's and the recipient's surface, respectively. The Ssb-Ypet foci were observed in one frame only, consistently with the 2.9-min lifespan of the ssDNA previously reported (27). Next, we combined a F-*parS* donor labeled

with AF-Mal^{488} and a recipient producing mCh-ParB to visualize the F pilus and the acquisition of the dsDNA plasmid by the recipient cell (Fig. 3*B*, *SI Appendix*, Fig. S2*B*, and Movie S10). Again, we observed that recipients, which were connected to a donor cell by an extended pilus, acquired the dsDNA plasmid as revealed by formation of a mCh-ParB focus. We note that mCh-ParB foci appeared in the vicinity of the pilus attachment point, consistent with the previous report that ssDNA-to-dsDNA conversion takes place at the location of plasmid entry (27). Next, we combined the three fluorescent reporter systems to perform three-color time-lapse imaging using a *ssb-ypet* donor labeled with AF-Mal^{488} and a recipient strain producing both Ssb-Ypet and mCh-ParB (Fig. 3*C*, *SI Appendix*, Fig. S3*C*, and Movie S11). This experiment recapitulates previous observations by allowing the successive visualization of the transfer of the ssDNA plasmid through the extended pilus, and its subsequent conversion into dsDNA within the recipient cells. All together, these time-lapse observations establish the existence of DNA transfer between cells that are solely connected by an extended pilus, which can bridge the physical gap between cells and act as a tube for the transport of the ssDNA molecule. We have quantified that these distant transfer events account for 6.4 ± 1.74% of all transfer events observed in the microfluidic chamber experiment (*SI Appendix*, Fig. S2*D*). Interestingly, we can note that distant plasmid transfer can occur through both straight and bent pili (Fig. 3).

Finally, we investigated whether the ability to transport DNA between physically distant cells was conserved for other F-like plasmids and during interspecies DNA transfer. Following the same experimental strategy as with *E. coli* F donors, we constructed a *S. enterica* strain carrying the F-like plasmid pED208, a derepressed derivative plasmid of the F_0Lac family (IncFV), first identified in *Salmonella* Typhi (32, 33), harboring a *parS* binding site and an expression plasmid (p *traA*^{T116C}) coding for a mutant TraA^{T116C} pilin for bioconjugation with fluorescent Maleimide (*SI Appendix*, Fig. S3*A*) (13). This diploid donor strain enabled efficient fluorescent labeling of pED208-encoded pili and exhibited conjugation efficiency comparable to the *wt* pED208 donor, both in the presence or the absence of maleimide labeling (*SI Appendix*, Fig. S3 *B* and *C*). Time-lapse imaging of pED208-*parS* conjugation in the microfluidic chamber was performed using a ParB-GFP-producing *E. coli* recipient strain (Fig. 3*D*). Analyses of ParB-GFP during time-lapse microscopy imaging revealed that *E. coli* recipient cells, which were only connected to an *S. enterica* donor cell by an extended pilus, acquired the dsDNA pED208 plasmid. This result supports that distant DNA transfer through the extended pilus is a conserved mechanism during conjugation of F-like plasmids (Fig. 3*D*).

Discussion

In this study, we used maleimide bioconjugation to fluorescently label and investigate spatiotemporal dynamics of the F pilus in living cells, thus providing valuable insights into the DNA transfer mechanism during bacterial conjugation. F pili were found to be anchored unevenly on the side of the donor cells, primarily near the midcell position and rarely in the polar region. This localization is remarkably reminiscent of the position of exit of the ssDNA from donor cells during F plasmid transfer (27), indicating that T4SS, which are active in pilus biogenesis and DNA transfer, are specifically rather than randomly positioned along the cell surface. This specific positioning pattern could reflect the nonrandom spatial arrangement of the T4SS machinery of the F plasmid within the cell, which is currently undocumented. Alternatively, if the T4SS machinery of the F plasmid were uniformly distributed along the cell periphery, similar to what has been observed for the pTi and R388 plasmids (34, 35), this pattern would strongly support the hypothesis that only the lateral T4SS pores are activated. This activation could be facilitated by the increased accessibility to F plasmid molecules, which are located at quarter positions within the cell and excluded from the cell poles (36, 37). Our results also corroborate previous studies using fluorescent phages (15, 29), demonstrating that the F pilus undergoes cycles of extension and retraction, even in the absence of recipient cells. Reversal events occur abruptly and randomly at any pilus length, with a highly variable time pattern. It is worth noting that the extension speed of the F pilus (49.5 nm/s) is relatively slow compared to other pili systems, such as *Vibrio cholerae* competence pilus (90 nm/s) (38) or the Tad Pili of *Caulobacter crescentus* (140 nm/s) (39). The moderate extension speed, combined with random extension-retraction cycles, pilus multiplicity, length, and flexibility, likely contribute to optimizing the ability of the F pilus to explore the cell's environment and increasing the probability of contacting a recipient cell. We can stress that although the majority of pili exhibit dynamic behavior, a subset remains nonretractile throughout the observation period. It is conceivable that the diverse dynamics of pili we have observed may arise from distinct stages of activation or molecular assembly between the pilus and the T4SS components, as documented through in situ CryoET methods (40). These varied assembly configurations could also play direct or indirect roles in the regulation of the multifaceted functions of the F pilus, such as attachment, aggregation, mating pair stabilization, plasmid transfer, and possibly even biofilm formation.

Importantly, our results show that pili encoded by the F and the pED208 F-like plasmids can serve as a conduit for DNA transport during conjugation between donor and recipient cells that are physically distant, thereby answering a long-standing and controversial question raised by Brinton almost 60 y ago (22, 23). This observation was possible thanks to the development of specific fluorescent reporter systems but also to the use of the microfluidics apparatus that offers several advantages. Unlike agarose-mounted microscopy slides, the microfluidic setup immobilized bacterial cells while allowing the pili to move freely on the cell sides. In addition, it was first reported by Dürrenberger et al. (17) and later confirmed by Clarke et al. (15) that the pilus retraction is associated with the rotation of the donor cell in relation to the recipient cell. However, cells immobilized within the microfluidic chamber are not able to rotate freely, which we think was critical to impede pilus retraction and enrich the microscopy fields of view with configurations where distant donor and recipient cells are connected solely by an extended pilus. Accordingly, this experimental setup provides the first direct observation of distant transfer via the F pilus, which was previously suggested by indirect evidence only (24, 25). Our findings also substantiate several inferences in favor of distant transfer made from structural data. The F pilus lumen diameter (28 Å) is large enough to accommodate for the passage of the ssDNA molecule attached to the TraI relaxases, which is unfolded during the passage through the T4SS (41, 42). Furthermore, while the exact conformation of the T4SS during transfer (40) and the route of the DNA through the T4SS machinery remains largely elusive, recent discoveries support the idea that the physico-chemical environment within the lumen is compatible with DNA transport. Indeed, work by Costa et al. (12) demonstrates that the alpha2-alpha3 loops of the TraA pilin project toward the lumen of the pilus and would be in contact with the translocated DNA. They also demonstrate that each TraA pilin composing the F pilus is associated with a phosphatidylglycerol (PG) molecule, the head of which is exposed to the pilus limen. These PG molecules are proposed to render the lumen's electrostatic potential

electronegative, thereby facilitating the transport of the ssDNA through the pilus.

Our work allows us to propose a unique model for bacterial conjugation. We suggest refining the term "contact-dependent" traditionally used to depict DNA conjugation, by introducing the terms "tight transfer" and "distant transfer". Tight transfer occurs either when bacteria are initially in cell-to-cell contact or after pilus attachment to the recipient cell resulted in complete retraction. Tight transfer is likely the most efficient conjugation pathway, as the establishment of cell-to-cell contact is followed by the stabilization of shearing force-resistant mating pairs through the interaction between the TraN protein exposed on the donor cell surface and the recipient's outer membrane protein OmpA (21). Alternatively, when pilus attachment cannot be followed by complete retraction, a distant transfer may occur through an extended F pilus. These findings highlight a unique role for the F pilus and emphasize the flexibility and adaptability of plasmid conjugation mechanisms, potentially expanding our understanding of how genetic material is exchanged between bacteria in diverse environments. The balance between tight and distant transfer would likely be influenced by factors such as medium properties and cell density, both in laboratory conditions and in natural ecosystems. Enterobacteriales carrying F-like plasmids primarily reside in the intestines of vertebrates, where they are surrounded by viscoelastic intestinal mucus that constrains bacterial movement. In these conditions, distant transfer through extended pili is likely physiologically relevant to compensate for the inability to establish direct contact between the mating cells. Whether the ability to transport DNA is restricted to specialized pili, such as thin and flexible pili encoded by F-like plasmids, or whether this is a general property of conjugative pili remains to be addressed. It is also important to note that transfer via a pilus is highly unlikely to be a universal process in conjugation. In fact, in Gram-positive bacteria, the mechanism of conjugation differs significantly from Gram-negative counterparts, as pili are not detected, and there is no formation of a specialized bridge connecting mating pairs of bacteria through a conjugative pilus.

The existence of both tight and distant transfer has implications regarding the regulation and molecular mechanism of F-like plasmids conjugation. It is well established that DNA transfer is triggered upon contact with the recipient bacterium, via a signal which nature remains unknown. While our findings do not uncover the exact nature of this signal, they do establish that wall-to-wall contact between donor and recipient cells is not essential for initiating DNA transfer. Instead, it is conceivable that the signal for transfer initiation is transmitted through a pilus-dependent mechanosensing mechanism, activated either by complete pilus retraction or when pilus retraction is hindered. Additionally, although our data demonstrate the ability of pili to transport DNA, existing literature consistently reports that extended F pili are dispensable for conjugation when stable wall-to-wall cell interactions are present. Donors lacking detectable pili can still perform plasmid transfer and often exhibit efficient conjugation under solid conditions (13, 43). This indicates that the production of surface-exposed pili is not required for transfer, as long as stable donor-recipient contact is facilitated. While extended pili are not required for conjugation, the TraA pilin subunit remains essential for conjugation in all tested conditions. The existence of TraA fibers that are not extended extracellularly but have exposed tips at the cell surface has been proposed from early experiments by Novotny and Fives-Taylor (44). They demonstrated that pili disassembly induced by NaCN hinders the adsorption of R17 bacteriophage to the sides of the pili but do not affect the adsorption of M13 phage to the pili tips. Therefore, it is possible that, even during tight transfer between closely apposed cells, the presence of very short "vestigial" pili is necessary for conjugation. Such rudimentary TraA polymers located within the T4SS system spanning the periplasm could make contact with the recipient cell's surface and potentially play a critical role in transporting the DNA through the conjugation pore during transfer.

Materials and Methods

Bacterial Strains and Plasmids. Bacterial strains used in this study are listed in *SI Appendix*, Table S1, plasmids in *SI Appendix*, Table S2, and oligonucleotides in *SI Appendix*, Tables S3. Construction of plasmids for the F-pilus labeling is described in Goldlust et al. (16). Briefly, to construct TraA single-mutant proteins (TraA^{S54C}), the *traA* gene amplified from the F plasmid was inserted into the pTrc99a expression plasmid by Gibson assembly. Substitution of the serine 54 by the cysteine was done by in vivo assembly mutagenesis directly on the pTrc99a *traA* (p *traA*). The pTrc99a *traA*^{S54C} plasmid (p *traA*^{S54C}) was then transformed into the *wt E. coli* K12 MG1655 carrying the F-Tn*10* plasmid to produce the partial diploid donor strain used for pilus labeling with fluorescent Maleimides. Genetic modifications of the F-Tn10 plasmid or the *E. coli* chromosome were performed by λRed recombination (45, 46). Modified F plasmids were transferred to the background strain K12 MG1655 by conjugation. When necessary, the *aph* and *cat* genes were removed using site-specific recombination induced by expression of the Flp recombinase from plasmid pCP20 (46). Cells were grown at 37 °C in Luria-Bertani (LB) broth medium or M9 supplemented with 0.2% casamino acids and 0.2% yeast extract. When appropriate, supplements were used at the following concentrations; Streptomycin 20 μg/mL, Ampicillin 100 μg/mL, Kanamycin 50 μg/mL, and Tetracycline 10 μg/mL and isopropyl β-D-1-thiogalactopyranoside (IPTG) 40 μM. Strains and plasmids were verified by Sanger sequencing (Eurofins Genomics).

Conjugation Assays. Overnight cultures in LB of recipient and donor cells were diluted to an OD_{600} of 0.05 and grown until OD_{600} ~ 0.8 was reached. Then, 25 μL of donor and 75 μL of recipient cultures were mixed (1:3 ratio) into an Eppendorf tube and incubated for 60 min at 37 °C. Conjugation mix was then vortexed, serial diluted, and plated on LB agar supplemented the appropriate antibiotic to select for donor (D), recipient (R), or transconjugant (T) populations. Conjugation efficiency is estimated by calculating the frequency of transconjugants (T/R+T).

F Pilus Labeling, Live-Cell Microscopy, and Image Acquisition. Labeling of *E. coli* F donors pili was performed as described in Goldlust et al. (16). Briefly, the overnight culture was diluted (1/100) in 5 mL of fresh LB without antibiotic and incubated at 37 °C with agitation to OD_{600} ~ 0.4. Then, 100 μL of the donor cell sample was mixed with 1 μL of Alexa Fluor 488 C5-maleimide (AF-Mal^{488}) or AF594 C5-maleimide (AF-Mal^{594}) (50 μg/mL) and incubated for 30 min at 37 °C without agitation. Cells were then gently centrifuged (1 min at 2,500 g) as washed in 100 μL of Rich Defined Medium (Teknova). The resulting prelabeled cell sample was either used directly for microscopy imaging of the donor alone or mixed in a ratio 1:1 with the recipient culture (OD_{600} ~ 0.8) for microscopy imaging of conjugation. Time-lapse imaging in a microfluidic chamber was performed as previously described (26, 27, 47) by loading the cell samples (donor alone or conjugation mix) into a B04A microfluidic chamber (ONIX, CellASIC®). Images were acquired with 10 s, 1 min, or 3 min/frame time intervals. The temperature was maintained at 37 °C during imaging. Snapshot microscopy was done using agarose-mounted slides prepared as in Lesterlin and Duabrry, 2016 (48). Then, 10-μL samples of cell culture were spotted onto 1% agarose pad and imaged directly into the thermostatic chambers maintained at 37 °C. Conventional wide-field fluorescence microscopy imaging was carried out on an Eclipse Ti2-E microscope (Nikon), equipped with ×100/1.45 oil Plan Apo Lambda phase objective, ORCA-Fusion digital CMOS camera (Hamamatsu), and using NIS software for image acquisition. Acquisitions were performed using 50% power of a Fluo LED Spectra X light source at 488 nm and 560 nm excitation wavelengths. For time-lapse experiment, exposure settings were 100 ms for Ypet, AF-Mal^{594}, AF-Mal^{488}, and mCherry, 50 ms for phase contrast. For snapshots experiments, exposure settings were 300 ms for AF-Mal^{594} and AF-Mal^{488}, 100 ms for Ypet, and mCherry.

pED208 Pilus Labeling, Live-Cell Microscopy, and Image Acquisition. For time-lapse imaging of conjugation between *S. enterica* pED208 donors and *E. coli* recipients, cultures were grown overnight and diluted (1/100) separately in fresh M9 supplemented with 0.2% casamino acids and 0.2% yeast extract at incubated at 30 °C. After 1 h, the cultures were supplemented with 500 μM IPTG (for the induction

of ParB-GFP production in the recipient harboring the pALA2903 plasmid) and 0.05% arabinose (for the induction of TraAT116C production in the donor harboring pBAD-*traA*^{T116C} plasmid). Donor and recipient cultures were then mixed in a ratio 1:1 and loaded into a B04A microfluidic chamber (ONIX, CellASIC®) followed by injection of the growth medium supplemented with DyLight^{550}-coupled maleimide (DL^{550}-Mal) (ThermoFischer). Images were taken during the subsequent injection of growth medium without dye to wash out the fluorescence background. The temperature was maintained at 30 °C during imaging. Images were acquired with a 20 min/frame time intervals. For snapshot microscopy, *S. enterica* cultures were diluted 1:100 from overnight cultures grown in LB at 37 °C. Strains expressing *traA*$_{T116C}$ under the control of the pBAD promoter were induced with arabinose 0.05% after 1 h of incubation. After reaching mid-exponential phase, a 500 µL aliquot was supplemented with 10 µM STAR GREEN maleimide (Abberior), incubated at 37 °C at 300 rpm for 2 min, then centrifuged at 2,500 g for 2 min. The supernatant was discarded, and the cells were resuspended in 500 µL PBS. Cells were spotted on a microscopic slide and covered with a coverslip before immediate imaging. Conventional wide-field fluorescence microscopy imaging was carried out on a Zeiss Axio Observer Z1 inverted epifluorescence microscope equipped with 100× objective and a temperature-controlled chamber. Filters 38He GFP and 43 DsRed (Zeiss) were used with the following respective settings: 20%, 200 ms, 20% 200 ms, and 75% 200 ms.

Image Analysis and Pili Detection. Quantitative image analysis was done using Fiji software with MicrobeJ plugin (28). For snapshot and time-lapse images, cell outlines detection was performed automatically and verified using the Manual-editing interface. When needed, detection of individual cells on cropped images was done semiautomatedly using the Manual-editing interface, which allows to select for the cell to be monitored and automatically tracked and analyzed. Labeled pili were detected and analyzed using MicrobeJ 5.13×. Pilus medial axes were detected using a single path propagation algorithm. The starting points of each pilus were detected using a local maximum algorithm along the contour profile of the corresponding cell, and the consecutive points were determined by local propagation (as illustrated in *SI Appendix*, Fig. S1*B*). If needed, the medial axes of misdetected pili were manually corrected using the editing interface of MicrobeJ using the segmented-line selection tool of ImageJ. The resulting selections were then stored in the Roi Manager and imported in MicrobeJ using the Filament detection mode. The medial axis of each filament was then refined automatically using a transversal local maximum neighbor algorithm and used to compute the geometrical and topological properties of the filament, such as its length, width, sinuosity, curvature, and angularity (as illustrated in *SI Appendix*, Fig. S1*B*). The relative position of the filament was determined for the starting point and/or the consecutive points. The resulting pili localization parameters were automatically extracted and plotted using MicrobeJ. During the search for distant transfer events, we exclusively validated and scrutinized events that took place after the third frame in the time-lapse sequence. This approach ensures capturing the entirety of the transfer event, eliminating the possibility of including events that had already commenced or concluded before the imaging began.

Statistical Analysis. *P*-value significance was analyzed running specific statistical tests on the GraphPad Prism software. Pilus length, extension, and retraction data from quantitative microscopy analysis were extracted from the MicrobeJ interface and transferred to GraphPad. *P*-value significance was then performed using unpaired nonparametric Mann–Whitney two-sided statistical test. When required, *P*-value and significance are indicated on the figure panels and within the corresponding legend.

Data, Materials, and Software Availability. All data to understand and assess the conclusions of this research are available in the main text and supporting information. Raw microscopy data are available on FigShare (DOI: 10.6084/m9.figshare.24260800) (49).

ACKNOWLEDGMENTS. We thank the National BioResource Project and Coli Genetic Stock Center for providing strains, Laurent Terradot for helping the early development of the F pilus labeling method; Tiago R.D. Costa for providing pED208 and the *wt* p *traA* plasmid and Nelly Schropp for early involvement in the project and help in plasmid construction. This research was funded by the Foundation for Medical Research (FRM-EQU202103012587), the French National Research Agency (ANR-18-CE35-0008 and ANR-22-CE12-0032) to C.L.; and a Grand Challenge Initiative Global Health grant of the Berlin University Alliance (no. 113_MC_GH_MEL-BER_Erhardt_HU) to M.E.

1. J. Lederberg, E. L. Tatum, Gene recombination in *Escherichia coli*. *Nature* **158**, 558 (1946).
2. J. G. Lawrence, Gene transfer, speciation, and the evolution of bacterial genomes. *Curr. Opin. Microbiol.* **2**, 519–523 (1999).
3. C. M. Thomas, K. M. Nielsen, Mechanisms of, and barriers to, horizontal gene transfer between bacteria. *Nat. Rev. Microbiol.* **3**, 711–721 (2005).
4. M. Barlow, What antimicrobial resistance has taught us about horizontal gene transfer. *Methods Mol. Biol.* **532**, 397–411 (2009).
5. C. Virolle, K. Goldlust, S. Djermoun, S. Bigot, C. Lesterlin, Plasmid transfer by conjugation in gram-negative bacteria: From the cellular to the community level. *Genes (Basel)* **11**, 1239 (2020).
6. M. P. Garcillán-Barcia, A. Alvarado, F. de la Cruz, Identification of bacterial plasmids based on mobility and plasmid population biology. *FEMS Microbiol. Rev.* **35**, 936–956 (2011).
7. G. Koraimann, Spread and persistence of virulence and antibiotic resistance genes: A ride on the f plasmid conjugation module. *EcoSal Plus* **8**, 2–4 (2018).
8. C. Stephens *et al.*, F Plasmids are the major carriers of antibiotic resistance genes in human-associated commensal *Escherichia coli*. *mSphere* **5**, e00709-20 (2020).
9. T. Date, M. Inuzuka, M. Tomoeda, Purification and characterization of F pili from *Escherichia coli*. *Biochemistry* **16**, 5579–5585 (1977).
10. D. E. Bradley, Characteristics and function of thick and thin conjugative pili determined by transfer-derepressed plasmids of incompatibility groups I1, I2, I5, B, K and Z. *J. Gen. Microbiol.* **130**, 1489–1502 (1984).
11. W. Paranchych, L. S. Frost, The physiology and biochemistry of pili. *Adv. Microb. Physiol.* **29**, 53–114 (1988).
12. T. R. D. Costa *et al.*, Structure of the bacterial sex F pilus reveals an assembly of a stoichiometric protein-phospholipid complex. *Cell* **166**, 1436–1444.e10 (2016).
13. K. Kishida *et al.*, Contributions of F-specific subunits to the F plasmid-encoded type IV secretion system and F pilus. *Mol. Microbiol.* **117**, 1275–1290 (2022).
14. K. Daehnel, R. Harris, L. Maddera, P. Silverman, Fluorescence assays for F-pili and their application. *Microbiology* **151**, 3541–3548 (2005).
15. M. Clarke, L. Maddera, R. L. Harris, P. M. Silverman, F-pili dynamics by live-cell imaging. *Proc. Natl. Acad. Sci. U.S.A.* **105**, 17978–17981 (2008).
16. K. Goldlust, A. Couturier, L. Terradot, C. Lesterlin, Live-cell visualization of DNA transfer and pilus dynamics during bacterial conjugation. *Methods Mol. Biol.* **2476**, 63–74 (2022).
17. M. B. Dürrenberger, W. Villiger, T. Bächi, Conjugational junctions: Morphology of specific contacts in conjugating *Escherichia coli* bacteria. *J. Struct. Biol.* **107**, 146–156 (1991).
18. M. Achtman, Mating aggregates in *Escherichia coli* conjugation. *J. Bacteriol.* **123**, 505–515 (1975).
19. W. A. Klimke, L. S. Frost, Genetic analysis of the role of the transfer gene, traN, of the F and R100–1 plasmids in mating pair stabilization during conjugation. *J. Bacteriol.* **180**, 4036–4043 (1998).
20. W. A. Klimke *et al.*, The mating pair stabilization protein, TraN, of the F plasmid is an outer-membrane protein with two regions that are important for its function in conjugation. *Microbiology (Reading)* **151**, 3527–3540 (2005).
21. W. W. Low *et al.*, Mating pair stabilization mediates bacterial conjugation species specificity. *Nat. Microbiol.* **7**, 1016–1027 (2022).
22. C. C. Brinton, P. Gemski, J. Carnahan, A new type of bacterial pilus genetically controlled by the fertility factor of *E. coli* k 12 and its role in chromosome transfer. *Proc. Natl. Acad. Sci. U.S.A.* **52**, 776–783 (1964).
23. C. C. Brinton, The structure, function, synthesis and genetic control of bacterial pili and a molecular model for DNA and RNA transport in gram negative bacteria. *Trans. N. Y. Acad. Sci.* **27**, 1003–1054 (1965).
24. L. C. Harrington, A. C. Rogerson, The F pilus of *Escherichia coli* appears to support stable DNA transfer in the absence of wall-to-wall contact between cells. *J. Bacteriol.* **172**, 7263–7264 (1990).
25. A. Babic, A. B. Lindner, M. Vulic, E. J. Stewart, M. Radman, Direct visualization of horizontal gene transfer. *Science* **319**, 1533–1536 (2008).
26. S. Nolivos *et al.*, Role of AcrAB-TolC multidrug efflux pump in drug-resistance acquisition by plasmid transfer. *Science* **364**, 778–782 (2019).
27. A. Couturier *et al.*, Real-time visualisation of the intracellular dynamics of conjugative plasmid transfer. *Nat. Commun.* **14**, 294 (2023).
28. A. Ducret, E. M. Quardokus, Y. V. Brun, MicrobeJ, a tool for high throughput bacterial cell detection and quantitative analysis. *Nat. Microbiol.* **1**, 16077 (2016).
29. L. Harb *et al.*, ssRNA phage penetration triggers detachment of the F-pilus. *Proc. Natl. Acad. Sci. U.S.A.* **117**, 25751–25758 (2020).
30. M. Achtman, N. Kennedy, R. Skurray, Cell–cell interactions in conjugating *Escherichia coli*: Role of traT protein in surface exclusion. *Proc. Natl. Acad. Sci. U.S.A.* **74**, 5104–5108 (1977).
31. R. Reyes-Lamothe, C. Possoz, O. Danilova, D. J. Sherratt, Independent positioning and action of *Escherichia coli* replisomes in live cells. *Cell* **133**, 90–102 (2008).
32. B. B. Finlay, W. Paranchych, S. Falkow, Characterization of conjugative plasmid EDP208. *J. Bacteriol.* **156**, 230–235 (1983).
33. J. Lu *et al.*, Analysis and characterization of the IncFV plasmid pED208 transfer region. *Plasmid* **48**, 24–37 (2002).
34. J. Aguilar, T. A. Cameron, J. Zupan, P. Zambryski, Membrane and core periplasmic Agrobacterium tumefaciens virulence Type IV secretion system components localize to multiple sites around the bacterial perimeter during lateral attachment to plant cells. *mBio* **2**, e00218-11 (2011).
35. G. Carranza *et al.*, Monitoring bacterial conjugation by optical microscopy. *Front. Microbiol.* **12**, 750200 (2021).

36. H. Niki, S. Hiraga, Subcellular distribution of actively partitioning F plasmid during the cell division cycle in *E. coli*. *Cell* **90**, 951–957 (1997).
37. S. Gordon, J. Rech, D. Lane, A. Wright, Kinetics of plasmid segregation in *Escherichia coli*. *Mol. Microbiol.* **51**, 461–469 (2004).
38. C. K. Ellison *et al.*, Retraction of DNA-bound type IV competence pili initiates DNA uptake during natural transformation in Vibrio cholerae. *Nat. Microbiol.* **3**, 773–780 (2018).
39. C. K. Ellison *et al.*, Obstruction of pilus retraction stimulates bacterial surface sensing. *Science* **358**, 535–538 (2017).
40. B. Hu, P. Khara, P. J. Christie, Structural bases for F plasmid conjugation and F pilus biogenesis in *Escherichia coli*. *Proc. Natl. Acad. Sci. U.S.A.* **116**, 14222–14227 (2019).
41. D. Arutyunov, L. S. Frost, F conjugation: Back to the beginning. *Plasmid* **70**, 18–32 (2013).
42. M. Trokter, G. Waksman, Translocation through the conjugative type IV secretion system requires unfolding of its protein substrate. *J. Bacteriol.* **200**, e00615-17 (2018).
43. M. M. Panicker, E. G. Minkley, DNA transfer occurs during a cell surface contact stage of F sex factor-mediated bacterial conjugation. *J. Bacteriol.* **162**, 584–590 (1985).
44. C. P. Novotny, P. Fives-Taylor, Retraction of F pili. *J. Bacteriol.* **117**, 1306–1311 (1974).
45. D. Yu *et al.*, An efficient recombination system for chromosome engineering in *Escherichia coli*. *Proc. Natl. Acad. Sci. U.S.A.* **97**, 5978–5983 (2000).
46. K. A. Datsenko, B. L. Wanner, One-step inactivation of chromosomal genes in *Escherichia coli* K-12 using PCR products. *Proc. Natl. Acad. Sci. U.S.A.* **97**, 6640–6645 (2000).
47. J. Cayron, A. Dedieu-Berne, C. Lesterlin, Bacterial filaments recover by successive and accelerated asymmetric divisions that allow rapid post-stress cell proliferation. *Mol. Microbiol.* **119**, 237–251 (2023).
48. C. Lesterlin, N. Duabrry, "Investigating bacterial chromosome architecture" in *Chromosome Architecture*, M. C. Leake, Ed. (Springer, New York, 2016), pp. 61–72.
49. C. Lesterlin *et al.*, The F pilus serves as a conduit for the DNA during conjugation between physically distant bacteria. Figshare. https://doi.org/10.6084/m9.figshare.24260800.v15. Deposited 9 October 2023.